Raman scattering in C_{60} and alkali-metal-saturated C_{60}

Ping Zhou, Kai-An Wang, Ying Wang, and P.C. Eklund
Department of Physics and Astronomy, and Center for Applied Energy Research, University of Kentucky, Lexington, Kentucky 40506

M.S. Dresselhaus
Department of Electrical Engineering and Computer Science, Massachusetts Institute of Technology, Cambridge, Massachusetts 02139 and Department of Physics, Massachusetts Institute of Technology, Cambridge, Massachusetts 02139

G. Dresselhaus
Francis Bitter National Magnet Laboratory, Massachusetts Institute of Technology, Cambridge, Massachusetts 02139

R.A. Jishi
Department of Physics, Massachusetts Institute of Technology, Cambridge, Massachusetts 02139 and Department of Physics, California State University, Los Angeles, California 90032
(Received 7 November 1991)

Experimental results on Raman-scattering spectra of C_{60} and M_6C_{60} (M =K, Rb, and Cs) taken at room temperature are presented and discussed. The spectra for the M_6C_{60} compounds are all quite similar, and show only weak dependence on the alkali-metal mass or radius. Several of the fivefold degenerate H_g symmetry C_{60} lines are observed to split upon doping. Furthermore, the high-frequency lines associated with primarily tangential carbon atom motions are observed to down-shift relative to their position in C_{60}, whereas C_{60} modes that exhibit primarily radial character down-shift to a lesser degree, and in some cases even up-shift slightly upon doping. These observations are explained as a consequence of the interplay between (1) the charge-transfer dependence of the bond stretching and bond-bending force constants and (2) the electrostatic effects associated with the net negative charge on the C_{60} cluster.

I. INTRODUCTION

Recently it has been possible to prepare ordered solid films of C_{60} that are insulating[1–4] and also doped films that are superconducting.[5–9] Much interest in the phonon spectrum and in the electron-phonon coupling has been aroused by the relatively high T_c values that have been reported: alkali-metal-doped K_3C_{60} (T_c = 18 K),[5,6] Rb_3C_{60} (T_c = 29 K),[7] and $Rb_xCs_yC_{60}$ (T_c = 33 K).[8,9] In this paper we present observations of the Raman spectra for insulating C_{60} and M_6C_{60} films (M= K, Rb, and Cs) and the interpretation of these spectra. We conclude with a discussion of these observations based on symmetry considerations and expected mode softening and stiffening effects connected with charge transfer arising from the alkali-metal doping.

C_{60}-related materials have been reported to show a face-centered-cubic structure for solid C_{60} (Refs. 1, 10, and 11) and K_xC_{60} ($x \leq 3$);[12] a body-centered-tetragonal structure for K_4C_{60};[13] and a body-centered-cubic structure for solid K_6C_{60}.[14] The C_{60} and M_6C_{60} solids studied in this paper are regarded as cubic materials with a very highly symmetric molecule (either rotating or at some random orientational position) placed at each cubic lattice site.

The room-temperature Raman spectrum presented in Sec. II for solid C_{60} (in agreement with previous work[3]) shows 10 strong Raman lines, consistent with the 10 Raman-allowed ($2A_g+8H_g$) modes predicted for the isolated C_{60} molecule.[15] Collected in Table I are calculated frequencies for molecular C_{60} according to Negri *et al.*,[17] which exhibit the best agreement with experiment, and the calculations of Stanton and Newton[15] which provide another point of comparison, as well as an estimate of the percent radial character of the vibrational eigenmodes. The calculated frequencies associated with modes of primarily radial character ($\omega < 750$ cm^{-1}) are in good agreement with experiment, whereas the calculated mode frequencies with largely tangential character (i.e., $\omega > 1400$ cm^{-1}) are found to be noticeably higher than the experimental values.

Since the bonding requirements of every carbon atom in the C_{60} truncated icosahedral structure are fully satisfied, C_{60} is an insulator with an optical-absorption edge at 1.7–1.8 eV in the fcc film.[20] The weak coupling of the C_{60} molecules to one another in the fcc structure retains the insulating nature of the clusters. However, metallic behavior results from potassium doping through the partial filling of the lowest antibonding T_{1u} (or F_{1u}) states of C_{60} by charge transfer from the alkali-metal dopants.

The molecular vibrational modes of the C_{60} molecule are classified in terms of the icosahedral point group.

TABLE I. Experimentally observed Raman modes in pristine C_{60} and comparison to various calculations.

	Experiment			Model			
	This work[a]		Meijer *et al.*[b]	Negri *et al.*[c]	Stanton and Newton[d]	Wu *et al.*[e]	Weeks *et al.*[f]
Mode	cm^{-1}	I_{HV}/I_{HH}	cm^{-1}	cm^{-1}	cm^{-1}	cm^{-1}	cm^{-1}
A_g	1468.5(1.5)	0.10	1470	1442	1667(0.0)	1627.4	1830
A_g	493.0(2.5)	0.02	496	513	610(100.0)	547.6	510
H_g	1573.0(9.5)	0.52	1575	1644	1722(1.2)	1830.7	2085
H_g	1426.0(7.5)	0.44	1428	1465	1596(0.8)	1688.2	1910
H_g	1248(7.0)		1250	1265	1407(2.1)	1398.5	1575
H_g	1099(7.0)		1099	1154	1261(9.6)	1160.0	1292
H_g	772.5(9.0)	0.38	774	801	924(30.5)	779.8	828
H_g	708.5(7.5)	0.40	710	691	721(96.5)	552.4	526
H_g	430.5(5.5)	0.40	437	440	447(90.0)	427.9	413
H_g	270.0(4.2)	0.52	273	258	263(69.3)	272.0	274

[a] The full width at half maximum intensity in cm^{-1} is given as (FWHM).

[b] Reference 16.

[c] Reference 17.

[d] Reference 15. For this calculation the percent radial character of the eigenvectors is given in parentheses for each mode.

[e] Reference 18.

[f] Reference 19.

Since each carbon atom in C_{60} bonds to three neighbors as in graphite, it would appear that there is a close connection between the planar sp^2 trigonal bonding that occurs in graphite and the tangential bonding of carbons in the C_{60} molecule. A certain subset (namely the tangential displacements) of the normal modes of C_{60} is associated with the stretching of C–C bonds analogous to the "planar"-type vibrations of the graphitic network of carbon atoms.

The similarity in the bond lengths and bond angles of graphite as compared to C_{60} leads one to expect that the phonon frequencies in both systems should be similar. Indeed the high-frequency phonon modes associated with predominantly tangential[15] motion of the carbon atoms in the C_{60} molecules are observed to be very close in frequency to the E_{2u} (1590 cm^{-1}) and E_{2g_2} (1582 cm^{-1}) modes in graphite.[21] On the other hand, whereas the out-of-plane A_{2u} zone-center mode in graphite has a frequency of 868 cm^{-1}, the radial modes in C_{60} have frequencies in the range 270–780 cm^{-1}.[15,16,22] It thus appears that the radial modes in C_{60} are substantially down-shifted with respect to the out-of-plane modes in graphite, a phenomenon that results from the surface curvature in C_{60}.[23] This difference between graphite and C_{60} with regard to surface curvature has been explained in a simple way, as summarized below.[23]

To understand the influence of the curvature on the radial modes in C_{60}, we note that the three bonds connecting a carbon atom to the three nearest-neighbor carbons are not coplanar. Upon constructing the relevant sp hybrids on each atom, it is possible to calculate the restoring force on a carbon atom that has been given an infinitesimal radial displacement. This calculation is done by considering the change in the bond energy that results from such a displacement, to second order in the displacement. In general, a radial displacement of an atom causes a change in the bond energy due to the change in the length of the bond as well as a change in the relative orientation of the orbits whose overlap determines the bond energy.

The calculation[23] yields a radial force constant in C_{60} that is approximately 40% lower than the corresponding out-of-plane force constant in graphite. Numerically, with the out-of-plane mode in graphite at $\omega \sim 868$ cm^{-1}, the corresponding radial mode in C_{60} is estimated to be at $\sim$ 700 cm^{-1},[23] in good agreement with the experimental value for the H_g mode at 708 cm^{-1}, which is 97% radial[15] and does indeed involve atoms displaced radially with respect to each other. It should be noted that the comparison between the 868 cm^{-1} A_{2u} mode in graphite should not be made with the radial A_g mode in C_{60} at 493 cm^{-1}. The 493 cm^{-1} mode in C_{60} involves primarily bond-stretching displacements, so that adjacent atoms are vibrating radially, but in phase. However, the 868 cm^{-1} out-of-plane mode in graphite involves an interlayer motion of adjacent atoms in the same layer which are 180° out of phase.

The room-temperature Raman spectra presented in Sec. II for the alkali-metal-doped C_{60} show great similarities to that for the undoped C_{60}. This observation suggests that we can model the effect of the alkali-metal doping on the lattice modes of the C_{60} solid in a similar manner to the approach taken in carrying out the lattice-dynamics studies in intercalated graphite,[24,25] where the alkali metal interacts only weakly with the graphene sheets, so that the main effect of intercalation on the lattice modes is the charge transfer associated with the alkali metal intercalation.

The effect of this charge transfer is to cause an expansion of the C_{60} molecular diameter and consequently a softening of the intraball force constants that determine the frequencies of the vibrational modes. The Raman frequencies are very sensitive to this intraball expansion, which has been directly measured by structural studies,[12] and predicted theoretically.[26] The effect of charge transfer on the lattice has been examined by calculating the change in the bond energy induced by charge transfer (as is for example introduced by an alkali-metal dopant).[27]

Considering only nearest-neighbor interactions, the new equilibrium bond length is found from the change in bond energy, as well as the bond-stretching force constant corresponding to this new equilibrium length. The various terms entering the expression for the modified stretching force constant are then evaluated.[27] The theory treats all alkali-metal atoms in the same way, i.e., as a charge-transfer dopant, and details of the hybridization and M-C_{60} coupling are not included. This theoretical approach is supported by the experimental results, in that the observed mode softening is indeed not sensitive to the alkali-metal mass and electronic configuration. For M_6C_{60}, where M represents an alkali metal such as K, Rb, or Cs, the charge transfer from the alkali-metal atoms to the C_{60} molecules is believed to be complete and thus results in a net charge per C atom $f_c = 0.1e$. Using this value of f_c, the calculation[27] predicts a softening of the high-frequency tangential modes of $\Delta\omega/\omega_0 = -0.027$, corresponding to a lowering of the high-frequency A_g mode by ~ 40 cm^{-1}.

On the basis of charge transfer alone, the frequency of the A_g radial bond-stretching mode at 493 cm^{-1} is expected to decrease by approximately 10 cm^{-1} following the above arguments. Instead it is observed that the frequency of this A_g mode up-shifts by $5-9$ cm^{-1} (see Sec. II). A partial explanation for this effect has been given in terms of an electrostatic effect arising from the charge transfer[27].

By calculating the change in the radial electric field at the surface of the fullerene (treated as a sphere of radius R) with net charge transfer Q when the radius of the sphere changes by the radial displacement u during a lattice vibration, an expression for the change in the square of the mode frequency is obtained.[27] The electrostatic effect then produces a stiffening which more than compensates for the softening due to charge transfer. Thus the high-frequency tangential A_g mode, which does not experience any similar electrostatic effect, is expected to soften by about 2%, while the radial A_g mode is expected to stiffen somewhat.

II. RAMAN EXPERIMENTS

A. Experimental details

The C_{60} molecules were prepared by an ac discharge between graphite electrodes in 200 torr of He.[1] This discharge produced a carbon soot from which 15% fullerenes C_{60} and C_{70} were extracted. Soxhlet extraction with a toluene solvent was used to separate the fullerene mixture from the soot. Separation of C_{60} from the higher-molecular-weight fullerenes was accomplished using liquid chromatography (LC). The identity of the high-performance LC separated fractions was verified by comparison of uv-visible spectra with published results,[1] and the purity of the C_{60} materials was verified by high-performance liquid chromatography (HPLC). We estimate C_{70} impurities to be less than 2%.

C_{60} powder was obtained by heating a concentrated solution of C_{60} in toluene in an alumina crucible at 50 °C in a N_2 atmosphere, and then vacuum drying the powder at 250 °C for four hours. Pristine C_{60} films were deposited onto silicon (100) substrates by sublimation from the same crucible in a vacuum of $\sim 10^{-6}$ torr. Ellipsometry was used to measure the thickness of the C_{60} films on the silicon substrate.[20] The next step in the preparation process was the doping of the C_{60} film on the Si substrate with alkali metals. Alkali-metal doping was carried out in a sealed quartz tube (25 cm long × 1 cm diam.) which contained the C_{60} film/Si substrate sample and alkali metal at opposite ends of the tube. The films were maintained at a higher temperature (200 °C) than the alkali metal (M) (100 °C) to avoid condensation of the alkali metal on the film surface. The reactions were carried out for 1 h which produced a color change in the films from yellow-brown to silver-black and a ~ 36 cm^{-1} down-shift of the strongest Raman line of pristine C_{60} at 1468.5 cm^{-1} to 1432.5 cm^{-1} in the M_6C_{60} compounds. The ampoules were returned to the furnace for another hour under the same conditions and no further down-shift of the peak was observed. A few samples were left in the furnace for 24 h to verify that saturation doping had taken place. Thus we conclude that our doped films are saturated with alkali metal.

Raman spectra of the pristine and doped C_{60} films were taken at $T \simeq 300$ K using an Ar-ion laser. Brewster-angle back-scattering geometry[22] was used to optimize the scattered signal. Cylindrical focusing of low ($P <$ 30 mW) laser radiation (spot size: 0.2 × 1.0 mm^2) was necessary to prevent laser-induced damage to the C_{60} films. Because of their high reactivity in air or water vapor, M_xC_{60} films were studied in their Pyrex growth ampoules. Pristine C_{60} films were handled in air, but the spectra were collected with N_2 gas flowing over the surface of the film.

Duclos *et al.*[28] have reported that short-term exposure (~10 min) of solid C_{60} to 1 atm of O_2, or an ambient atmosphere, results in an up-shift of the charge-transfer-sensitive Raman mode (A_g) at 1458 cm^{-1} to 1468 cm^{-1}. This observation is consistent with the recent pressure-dependence study by Tolbert *et al.*[29] in which the zero pressure intercept is quite close to 1458 cm^{-1}. However, other authors[16,30] have reported values for this A_g mode in agreement with the present work. Work is in progress in our laboratory to further study the O_2 sensitivity of C_{60}.[31] Furthermore, Duclos *et al.*[28] report that the down-shifted A_g symmetry line in K_6C_{60} appears at 1432 cm^{-1} in good agreement with the present study, whether or not the pristine C_{60} sample was first exposed to O_2.

B. Experimental Raman results

In this section we give a more complete exposition of the Raman spectra than presented previously.[22] Figure 1 shows low-resolution (6 cm^{-1}) unpolarized Raman spectra of pristine C_{60} and M_xC_{60} where M=(K, Rb, Cs) and $x \approx 6$; all films were ~ 1000 Å in thickness.

Starting with the C_{60} spectrum reported by Bethune and Meijer,[30] 10 Raman lines ($2A_g + 8H_g$) are predicted from group theory[32] for an isolated molecule and 10

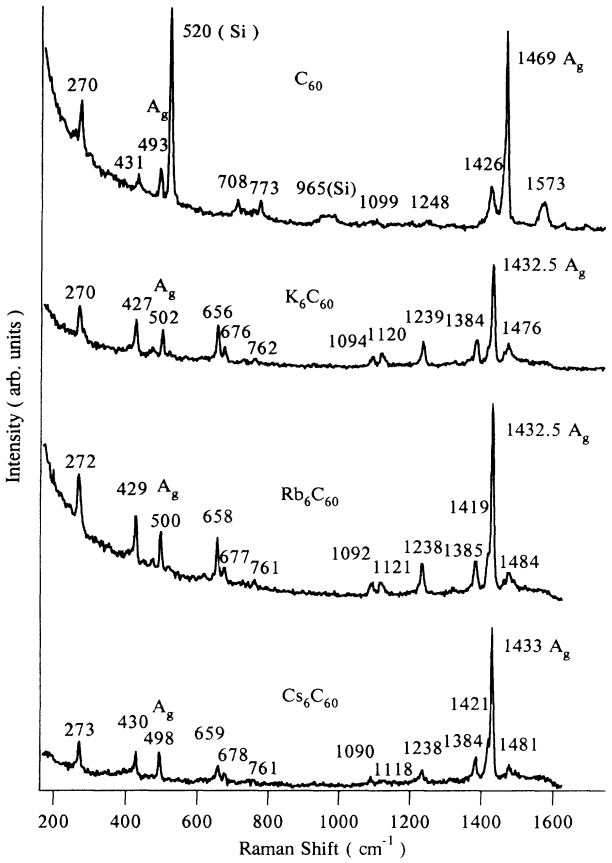

FIG. 1. Experimental Raman spectra for pristine C_{60}, K_6C_{60}, Rb_6C_{60}, and Cs_6C_{60}. The tangential and radial A_g modes are identified, as are features associated with the Si substrate.

strong lines are indeed observed. The features at 520 cm^{-1} and 965 cm^{-1} in Fig. 1 are due to the silicon substrate. The central frequencies and linewidths [full width at half maximum (FWHM)] of the ten Raman-allowed lines are listed in Table I. The mode frequencies are in good agreement with the recent results of Meijer *et al.*[16] also listed in the table. The FWHM linewidths are corrected for the spectrometer resolution and it is interesting to note that most of the lines are quite narrow ($2 < \text{FWHM} < 9$ cm^{-1}). In addition, the experimental results are compared in this table with those of 4 different calculations of the intramolecular modes of C_{60} and the best agreement is achieved with that of Negri *et al.*[17] Of interest to the interpretation of the experimental results is the amount of admixture of tangential and radial components in each of the C_{60} modes as calculated by Stanton and Newton,[15] and summarized in parentheses in Table I.

Referring to the spectra for the three M_6C_{60} samples in Fig. 1, we see almost the same spectrum, independent of whether the alkali metal is K, Rb, or Cs. Of particular interest also is the similarity of these three spectra to that for C_{60}. Several of the lines in the M_6C_{60} spectra down-shift in frequency relative to that for pristine C_{60}, and a few of the M_6C_{60} lines split. The small differences between the M_6C_{60} and C_{60} spectra are discussed in detail below, and are related to theoretical considerations published elsewhere.[32] To facilitate this comparison, we list in Table II the frequencies for Raman-active modes in C_{60} and in M_6C_{60} (where M=K, Rb and Cs) obtained in the present work, including the linewidths (FWHM) and the depolarization ratio I_{HV}/I_{HH}, where, for example, I_{HV} refers to the scattered intensity for incident and scattered light polarized, respectively, in the plane of incidence and perpendicular to the plane of incidence.

It should be remarked that the Raman line shape for all the modes in C_{60} and M_6C_{60} is observed to be Lorentzian and not Gaussian. A Gaussian line shape results from inhomogeneous broadening from a random distribution of defects, such as might arise from incomplete doping of M atoms or oxygen uptake. The Lorentzian line shapes observed here are therefore consistent with the view that intramolecular C-C interactions dominate the Raman-active vibrations. Lower-frequency Raman-active modes associated with intramolecular motion are anticipated,

TABLE II. Experimentally observed Raman modes in C_{60} and alkali-metal-doped C_{60}.

		C_{60}	K_6C_{60}		Rb_6C_{60}		Cs_6C_{60}	
I_h mode	T_h mode	cm^{-1}	cm^{-1}	I_{HV}/I_{HH}	cm^{-1}	I_{HV}/I_{HH}	cm^{-1}	I_{HV}/I_{HH}
A_g	A_g	1468.5	1432.5[3.0][a]	0.13	1432.5[2.7]	0.10	1433.0[2.0]	0.10
A_g	A_g	493.0	502.0[0.5]	0.10	499.5[0.4]	0.12	497.5[0.5]	0.11
H_g	$E_g + T_g$[b]	1573.0	1476.0[7.5]	0.48	1483.5[15]	0.80	1480.5[4.5]	0.54
H_g	$E_g + T_g$	1426.0	1383.5[6.0]	0.50	1419.5[11.0] 1385.0[8.7]	0.14 0.60	1421.0[6.5] 1384.0[4.5]	0.28 0.52
H_g	$E_g + T_g$	1248	1237.0[6.5]	0.88	1238.5[0.8]	0.57	1238.0[4.5]	0.44
H_g	$E_g + T_g$	1099.0	1120.0[6.5] 1094.0[5.5]	0.38 0.42	1120.5[12.0] 1092.0[11.0]	0.35 0.78	1118.0[11.0] 1090.0[8.5]	0.58 0.91
H_g	$E_g + T_g$	772.5	761.5[0.5]	0.75	760.5[2.0]	0.68	761.0[4.0]	0.50
H_g	$E_g + T_g$	708.5	676.0[0.5] 656.0[2.5]	0.00 0.49	676.5[–] 657.5[2.2]	0.00 0.74	678.0[0.5] 658.5[2.5]	0.00 0.47
H_g	$E_g + T_g$	430.5	427.0[0.5] 419.5[0.5]	0.71 0.75	428.5[–] 421.5[0.8]	0.65 0.61	429.5[–] 424.0[0.5]	0.63 0.87
H_g	$E_g + T_g$	270.0	281.0[2.0] 269.5[2.5]	0.91 0.71	277.0[0.7] 271.5[0.9]	0.85 0.54	272.5[0.5]	0.48

[a] Raman lines at 1430 cm^{-1} and 1447 cm^{-1} for $x = 6$ and $x = 3$, respectively, have been reported by Haddon *et al.* (Ref. 5).

[b] For the modes which show a splitting, the mode with the smallest value of I_{HV}/I_{HH} is identified with the E_g symmetry mode.

but have not been observed here.

Referring to the C_{60} spectrum, weak lines are observed at 1099 and 1248 cm^{-1} (see Fig. 2 for the upper part of the spectral range $1000 < \omega < 1600$ cm^{-1}) when the spectrum is taken at higher intensity. One might attribute these two weak lines to impurities. The persistence of these lines in the M_6C_{60} films at 1094 and 1237 cm^{-1}, respectively, suggest that they may be two of the 10 Raman-allowed modes, in agreement with the work of Meijer *et al.*[16] The features due to the silicon substrate at 520 and 965 cm^{-1} vanish in the doped films, consistent with a higher optical absorption near the laser wavelength (4880 Å) in M_6C_{60} as compared to pristine C_{60}. In the following, particular attention will be given to the two A_g modes, the high-frequency tangential A_g mode occurring at 1468.5 cm^{-1}, and the low-frequency radial A_g mode occurring at 493 cm^{-1} in pristine C_{60}.

The symmetry of the A_g lines is identified through polarization analysis of the Raman spectra, since the A_g modes are only seen for the (||, ||) polarization, while the H_g modes are Raman active for both (||, ||) and (||, ⊥) polarizations. In the low-resolution (6 cm^{-1}) polarized spectra of C_{60} and Rb_6C_{60} films in Fig. 3 we see two strongly polarized modes as noted above for C_{60}, and these modes are identified with A_g symmetry on the basis of the above-mentioned symmetry selection rules. These two modes remain strongly polarized in the spectrum for Rb_6C_{60}. In this figure the notation (H, H) denotes (||, ||), while (H, V) is used to denote (||, ⊥). We note that the radial A_g mode is very strongly polarized; i.e., $I_{HV}/I_{HH} = 0.02$. However, the tangential A_g mode polarization is only $I_{HV}/I_{HH} = 0.10$. Subsequent work at very low laser powers has shown a polarization ratio $I_{HV}/I_{HH} \sim 0.02$ for the tangential A_g mode.[33]

To check the stability of the M_6C_{60} samples under laser irradiation, spectra were taken as a function of laser power, as shown in Fig. 4 for Rb_6C_{60}. We find no laser-induced changes in the Raman spectra for the Rb_6C_{60} samples for power levels up to 320 mW.

The situation for C_{60} is different. The Raman spectra for C_{60} for various power levels up to 320 mW (see Fig. 5) show the growth of a feature near 1464 cm^{-1} with increasing laser power. The C_{60} film samples were handled in air, but measured under flowing N_2.

As mentioned above, Duclos *et al.*[28] have studied the influence of oxygen on the Raman spectra of C_{60} films and have concluded that their Raman peak at 1467 cm^{-1} is somehow associated with the presence of oxygen in the ampoule. A lower-frequency peak at 1458 cm^{-1} is identified by Duclos *et al.* as the intrinsic A_g tangential C_{60} line. Thus on the basis of the work of Duclos *et al.*,[28] potassium addition down-shifts the tangential A_g mode by 4.3 cm^{-1}/K unit as compared with a down-shift of 6.0 cm^{-1}/K unit when reference to the zero charge state is made to a line in C_{60} at 1469 cm^{-1}.[28] Overall, the Raman spectrum of C_{60} reported by Duclos *et al.*[28] is similar to the results reported here. However, Duclos *et al.* reported 6 additional lines which were not observed in our samples. The radial mode frequencies agree better with the data reported here than do the values of the

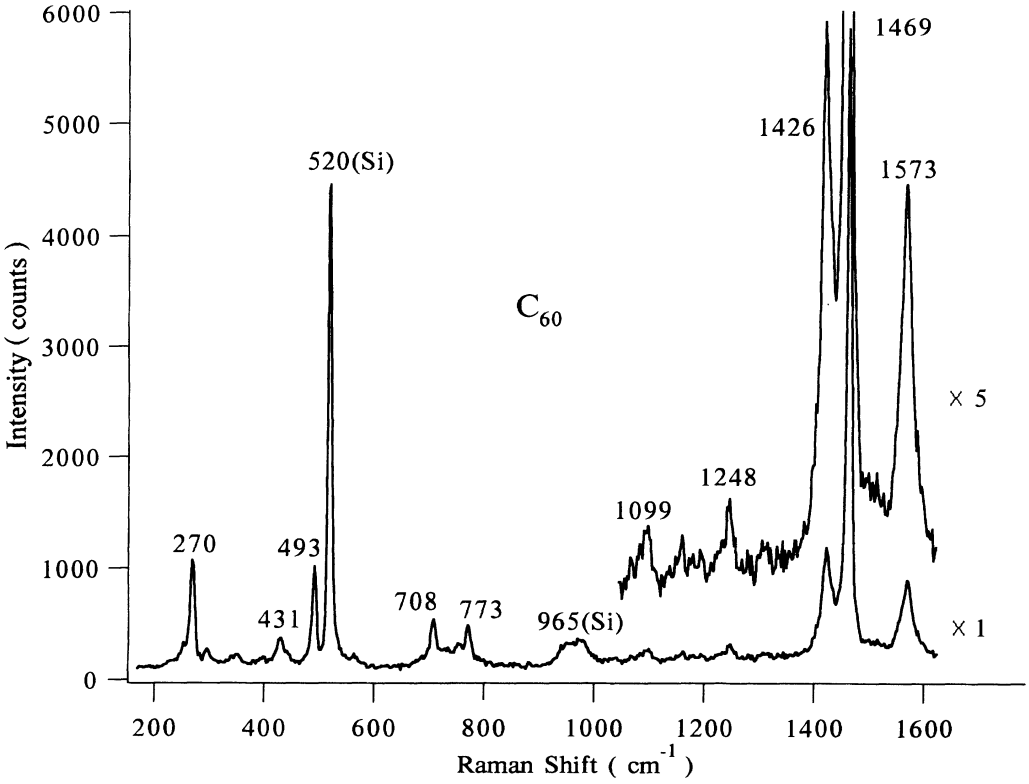

FIG. 2. Experimental Raman spectrum for pristine C_{60} shown in more detail. The 10 Raman-allowed modes are identified, as are the features associated with the Si substrate.

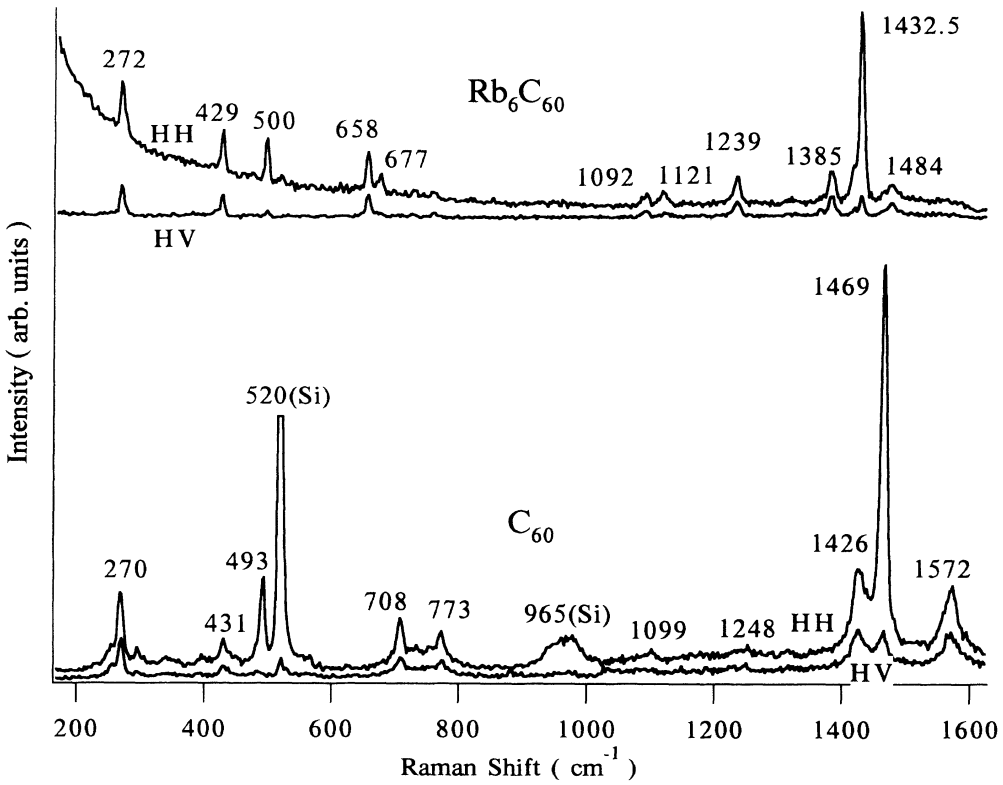

FIG. 3. Polarized Raman spectrum for Rb_6C_{60} in comparison to that for C_{60} (see text).

higher-frequency tangential modes. Further work is underway in our laboratory to study the effect of oxygen exposure on the C_{60} film properties.[31]

The various features of the spectrum for Rb_6C_{60} in Fig. 1 are shown under higher resolution in Fig. 6. The evolution of the two A_g modes in pristine C_{60} after Rb doping are shown in Figs. 6(c) and 6(h), where it is seen that the strong polarization selection rule of the pristine C_{60} is retained after Rb doping to Rb_6C_{60} for both the radial A_g mode (which is up-shifted from 493.0 cm^{-1} to 499.5 cm^{-1}) and the tangential A_g mode (which is down-shifted from 1468.5 cm^{-1} to 1432.5 cm^{-1}, in agreement with Haddon *et al.*[5]).

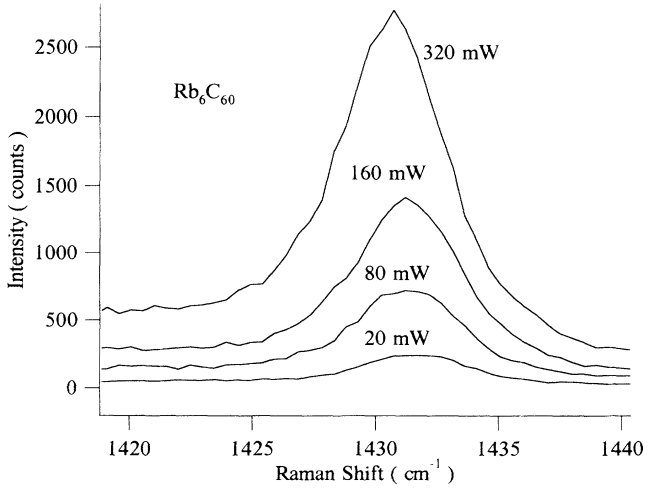

FIG. 4. Raman spectrum for Rb_6C_{60} taken at various incident laser intensities.

The dependence of the Raman-active H_g- and A_g-derived mode frequencies on alkali-metal doping can be understood by reference to the following observations.

(1) The bond-stretching force constants decrease as a result of lattice expansion.

(2) There is an even larger decrease in the bond-angle-bending force constants as a result of this lattice expansion.[23]

(3) Modes with dominantly radial character are less down-shifted in frequency than modes with dominantly tangential character. In fact, the radial A_g breathing mode is actually up-shifted in frequency as explained in Ref. 23 and in Sec. I.

Thus in determining the effect of doping on the different modes, it is important to consider the radial or tangential character of the mode as far as the atomic displacements are concerned, especially the magnitude of the contribution of the angle-bending force constants to the normal mode. Such information is partially supplied by Stanton and Newton.[15]

The high-resolution data of Fig. 6 show that some of the C_{60} modes split, while others do not, such as the H_g mode at 1248 cm^{-1} which down-shifts by 9.7 cm^{-1} to 1238.5 cm^{-1} in Rb_6C_{60} [see Fig. 6(g)] and the H_g mode at 772.5 cm^{-1} in C_{60} which down-shifts by 12 cm^{-1} to 760.5 cm^{-1} in Rb_6C_{60} [see Fig. 6(e)]. Both lines [Figs. 6(e)

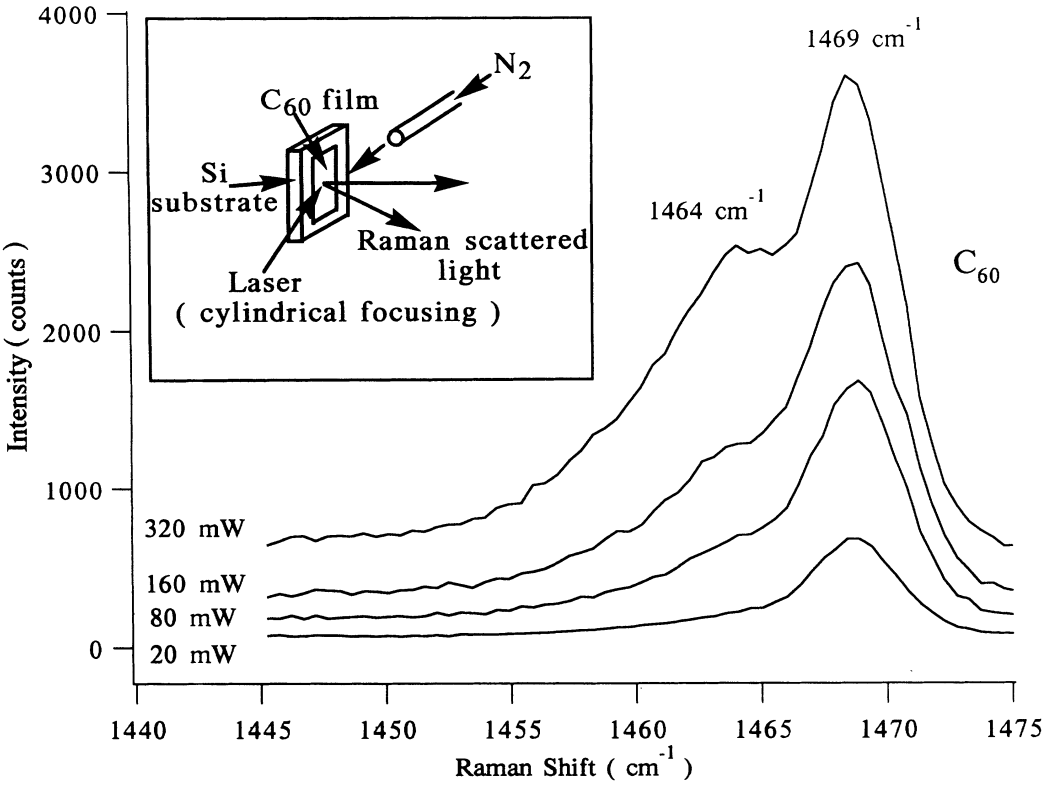

FIG. 5. Raman spectrum for pristine C_{60} taken at various incident laser intensities. The inset shows the geometry used for these measurements. Cylindrical focusing is employed and the measurements are made under flowing nitrogen gas. Under rigid exclusion of O_2, the shoulder at 1464 cm^{-1} grows at the expense of the 1469 cm^{-1} line and downshifts to 1460 cm^{-1}.[31]

and 6(g)] show essentially no dependence on alkali-metal species. For the H_g modes at ~1384 cm^{-1} and 1480 cm^{-1} in the M_6C_{60} samples, no splitting nor dependence on alkali-metal species is observed.

The group-theoretical analysis reported elsewhere[32] shows that the reduction of the symmetry from I_h (isolated molecule) to T_h results in the splitting of all H_g-derived modes into a two-dimensional E_g mode and a three-dimensional T_g mode. The polarization selection rules are different for each of these symmetries. The H_g mode has Raman tensor components for both $(\|,\|)$ and $(\|,\perp)$ scattering; however the E_g mode only shows $(\|,\|)$ scattering and the T_g mode shows only $(\|,\perp)$ scattering. The four-dimensional G_g and G_u modes in icosahedral symmetry also split into a one- and three-dimensional mode in T_h symmetry. Furthermore, all even parity modes become Raman active, thus predicting 37 Raman modes.[32]

Examples of C_{60} Raman lines that split under Rb doping to Rb_6C_{60} are seen in Figs. 6(a), 6(b), 6(d) and 6(f). In two cases [Figs. 6(a) and 6(b)] the splittings are small and no polarization sensitivity is observed. In contrast, for the two cases shown in Figs. 6(d) and 6(f), the splittings of the H_g modes are much larger than for Figs. 6(a) and 6(b). For the spectra in Figs. 6(d) and 6(f), we further see a strong polarization sensitivity for the higher-frequency component. The lines in Figs. 6(d) and 6(f) are not A_g, and we assume they are E_g symmetry. We now discuss each of the frames in Fig. 6 in more detail.

The lowest-frequency intramolecular mode in C_{60} at 270 cm^{-1} (see Table II) shows a small up-shift in frequency and a splitting upon Rb doping [Fig. 6(a)], but no polarization-sensitive behavior. An up-shift of ~2.5 cm^{-1} (or ~1%) is observed for the average of the central frequencies of the two components relative to the corresponding line in C_{60}, and this up-shift seems to be approximately independent of mass of the alkali-metal dopant, thus suggesting that this effect arises predominantly from charge transfer. The small magnitude of the species-dependent effect indicates a weak coupling between each fullerene and the surrounding alkali-metal ions.

With regard to the line at 430.5 cm^{-1} in C_{60} [see Fig. 6(b)], the splitting in Rb_6C_{60} is 7.0 cm^{-1} (or 1.6%) and the splitting decreases with the mass of the alkali-metal dopant. Both components of the Rb_6C_{60} lines are down-shifted relative to C_{60} and the mean position is down-shifted by 5.5 cm^{-1} (or ~ 1%). This down-shift decreases with increasing alkali-metal mass. From the calculation of Stanton and Newton[15], the modes at 270 cm^{-1} and 430.5 cm^{-1} are both predominately radial in character, with the higher-frequency mode having more radial character than the lower-frequency mode. The contribution of the angle-bending force constants to the higher-frequency mode is expected to be larger than to the low-frequency mode, thus accounting for the

larger mode softening for the upper-frequency mode due to charge-transfer effects.

On the other hand, the radial A_g mode which occurs at 493.0 cm^{-1} in C_{60} is up-shifted by 6.5 cm^{-1} (or 1.4%) in Rb_6C_{60} [Fig. 6(c)] and the up-shift decreases with increasing alkali-metal mass; this observation is generally consistent with the explanation by Jishi and Dresselhaus[27] in terms of charge transfer and electrostatic effects, though the observed up-shifts somewhat exceed the theoretically estimated values.[27] Although the fullerene expansion (resulting from charge transfer) causes the bond-stretching force constant to decrease, the variation in the electric field at the sites of the charged carbon atoms as they vibrate radially produces an opposite effect, namely, an increase in the bond-stretching force constant. The fact that the observed up-shifts somewhat exceed those calculated on the basis of this argument, and that these up-shifts decrease with increasing alkali-metal mass indicates that the interaction between the negatively charged fullerene and the alkali-metal ions does contribute to the stiffening effect, but the magnitude of that contribution is very difficult to calculate.

The next highest frequency mode at 708.5 cm^{-1} in C_{60} is a predominantly radial mode that splits and signifi-

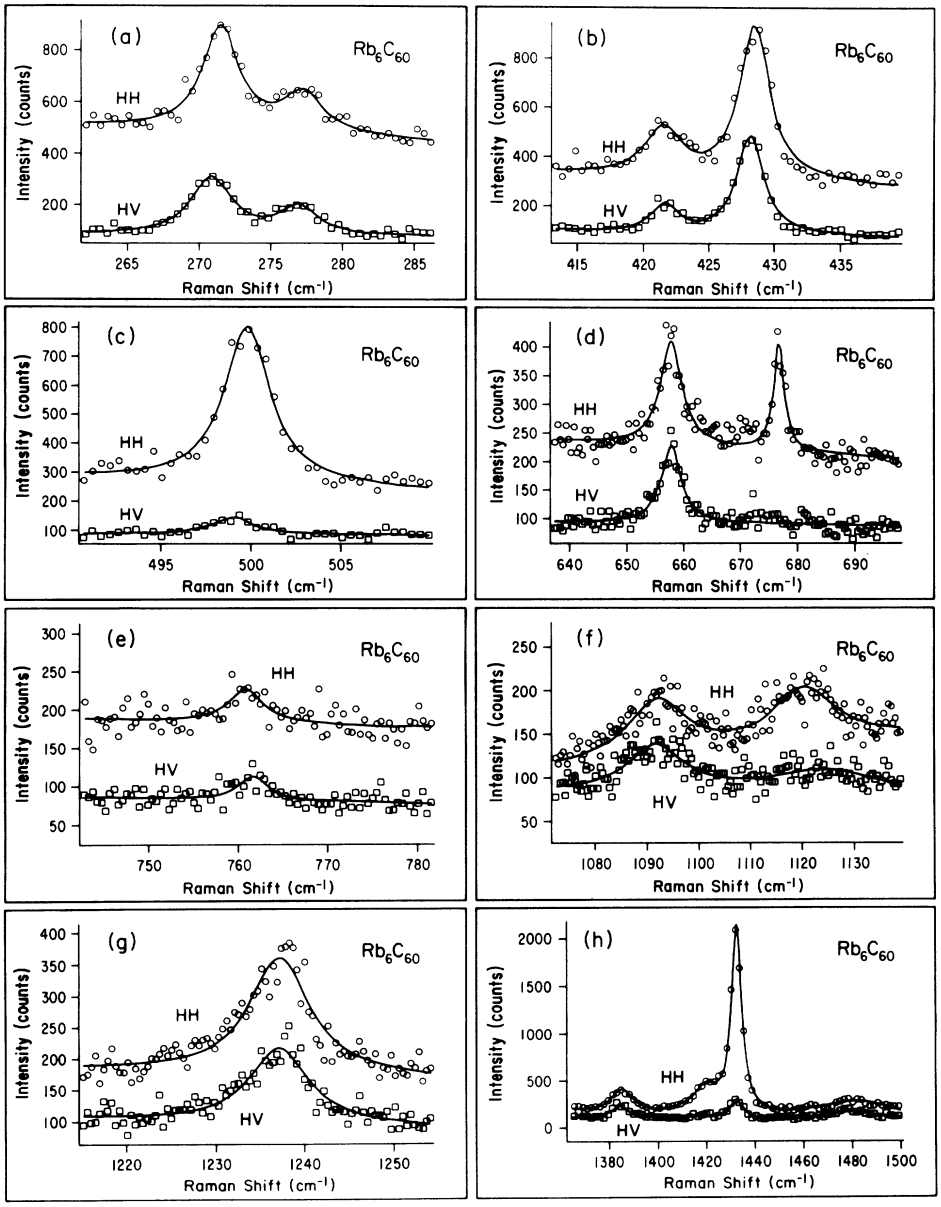

FIG. 6. Higher-resolution ($\sim$ 2.5 cm^{-1}) detailed spectra for Rb_6C_{60} for light polarized in the plane of incidence (H or $\|$). The scattered light is polarized either parallel (H or $\|$) or perpendicular (V or $\perp$) to the incident light. Each of the Raman lines in Table I is shown. Of interest is the difference in splitting and polarization properties for the various lines. The various features are shown in detail in the eight panels.

cantly down-shifts on alkali-metal doping [see Fig. 6(d)]. Of particular interest here is the strong polarization effect associated with the upper-frequency component of the doublet, which is identified with E_g symmetry. For Rb_6C_{60}, the splitting is 19.0 cm^{-1} (or 2.7%), but in this case, the splitting is independent of the mass of the alkali-metal dopant, as is also the down-shift of the lines. Also for this case there are large down-shifts in the frequency of the average of the two Rb_6C_{60} lines relative to the C_{60} line (41 cm^{-1} or 5.8%). Although no quantitative explanation of the large shifts observed for this predominantly radial mode is presently available, we can nevertheless offer a qualitative explanation based on the above discussion. According to Stanton and Newton,[15] the rms variation in the bond stretching of the C–C bond per unit variation of normal coordinate is 0.004, while for the C=C double bond it is essentially zero; however, for the angle bending of the C–C–C and C–C=C bonds it is 5.7°/Å and 4.5°/Å, respectively. This indicates that the angle-bending force constants make an appreciable contribution to the frequency of the H_g mode in C_{60} at 772.5 cm^{-1}. Since the angle-bending force constant is appreciably decreased by charge transfer, there is a correspondingly large down-shift in the frequency of this mode upon doping. A precise estimate would, of course, require carrying out a detailed lattice-dynamical calculation.

The Raman mode, which for C_{60} is observed at 772.5 cm^{-1}, is observed to down-shift by 12 cm^{-1} (or 1.5%) in Rb_6C_{60} [see Fig. 6(e)]. Neither splitting nor dependence on alkali-metal mass is observed for this line, which furthermore shows no important polarization effects. The small down-shift in frequency may be due to charge-transfer effects, somewhat reduced by electrostatic effects associated with the partial radial character of this mode.

In the vicinity of 1100 cm^{-1}, two lines are found in Rb_6C_{60} [see Fig. 6(f)] split by 28.5 cm^{-1} and these features are also found in the spectra for K_6C_{60} and Cs_6C_{60} at essentially the same frequencies. In all spectra the upper-frequency line shows some polarization effects, with a stronger signal observed for the $(\|, \|)$ or (H, H) geometry relative to $(\|, \perp)$ or (H, V). The average of the two lines for this dominantly tangential mode up-shifts by 7 cm^{-1} relative to the corresponding feature in C_{60}. We have as yet no explanation for this effect.

The predominantly tangential mode at 1248 cm^{-1} in C_{60} down-shifts by 9.5 cm^{-1} (or 0.8%) in Rb_6C_{60} [see Fig. 6(g)]. No line splitting is observed nor is a dependence found on the mass of the alkali metal. Since the mode predominantly involves tangential displacements, the dependence of the mode frequency on alkali-metal mass is expected to be small, consistent with the weak-fullerene–alkali-metal coupling.

Finally in Fig. 6(h) we see the remaining modes in Rb_6C_{60}. The mode which occurs in C_{60} at 1426 cm^{-1} appears to split into two modes separated by 34.5 cm^{-1} (or 2.4%), with the upper-frequency line strongly polarized, and identified with E_g symmetry. The down-shift of the average of this pair of lines is 23.8 cm^{-1} (or 1.7%), presumably associated with the mode softening that occurs in the tangential modes due to the charge transfer.

We attribute the dominant line at 1432.5 cm^{-1} in the Rb_6C_{60} spectrum to the tangential A_g mode on the basis of its polarization dependence, and we identify this feature with the line at 1468.5 cm^{-1} in C_{60}, corresponding to a softening of 36 cm^{-1}. The mode softening of this tangential A_g mode is well explained by charge transfer,[27] causing an expansion of the fullerene, which in turn induces a softening of the bond-stretching force constant whose value determines the frequency of this A_g mode. This effect is very similar to that observed in intercalated graphite.[21]

Neither splitting nor polarization effects are observed for the highest-frequency line in the spectra for the alkali-metal-doped samples. This line appears in Rb_6C_{60} at 1483.5 cm^{-1}, and within experimental error, is independent of the mass of the alkali dopant. With regard to the identification of this line in the doped samples with those in the C_{60} spectrum, we refer to Fig. 1, where we see a distinctive pattern for the high-frequency portion of all four spectra shown in this figure. On this basis, we identify the highest-frequency mode in the doped samples with the tangential H_g mode at 1573 cm^{-1} in the C_{60} spectrum. A more detailed study as a function of alkali-metal concentration is needed to confirm this assignment. The large doping-induced down-shift of $\sim$90 cm^{-1} for this line in the doped Rb_6C_{60} spectrum is anomalously high relative to that observed in the behavior of the other predominantly tangential modes in the spectrum. However, it can be explained simply by noting that the angle-bending force constants make an especially large contribution to the frequency of this mode, as indicated by the rms values given by Stanton and Newton.[15] Actually, this mode is the most sensitive among all the Raman-active modes to the variation in the angle-bending force constants,[15] and consequently, the down-shift in the frequency of this mode should therefore be expected to be the highest.

Most of the features in the high-resolution spectra in Fig. 6 show very little dependence on the alkali-metal species as indicated in Table II. The few features that do show such an alkali-metal dependence are the radial A_g mode (at 493 cm^{-1} in C_{60}) and the doublet components corresponding to the two H_g modes (at 270 cm^{-1} and 430.5 cm^{-1} in C_{60}), both of which are also predominantly of radial character. The alkali-metal dependence of the radial A_g mode can be accounted for by assuming that the electrostatic interaction between the alkali metal and fullerene causes a mode stiffening which is most pronounced for K_6C_{60} where the nearest-neighbor distance between the metal and carbon atoms is smallest.[18]. On physical grounds, one would expect the alkali-metal dependence to be more pronounced for vibrations involving predominantly radial displacements, in agreement with observations. The alkali-metal dependence of the upper frequency component of the doublet associated with the 270-cm^{-1} H_g mode may have a similar explanation. To account for the smaller alkali-metal dependent shifts associated with the three other doublet components in Figs. 6(a) and 6(b) at 271.5 cm^{-1}, 421.5 cm^{-1}, and 428.5 cm^{-1} in Rb_6C_{60}, a more detailed lattice-dynamical cal-

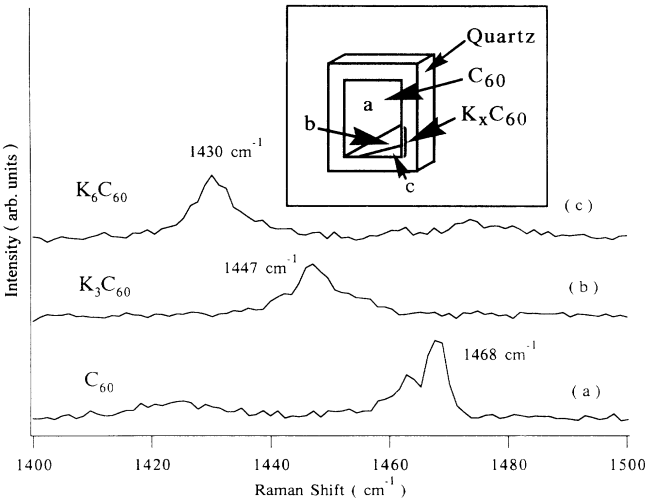

FIG. 7. Raman spectra taken in regions (a), (b), and (c) for a K_xC_{60} film on a quartz substrate with a potassium concentration gradient between region (a) (pure C_{60}) to region (c) (K_6C_{60}), as indicated in the inset. The spectra shown are typical of a number of spectra taken in regions (a), (b), and (c).

culation for the normal modes will be needed.

A study of the Raman spectra as a function of alkali metal concentration was carried out at low laser power (< 30 mW) for frequencies between 1400 and 1500 cm^{-1} using a C_{60} film on a quartz substrate for which the doping process was terminated before the saturation had occurred. The doping apparently was initiated at one corner of the sample (see inset to Fig. 7). Raman spectra were taken for several spots in each of regions (a), (b), and (c) along the concentration gradient. The Raman spectra show three distinct spectra, as illustrated in Fig. 7. Raman scans for region (a) yielded a spectrum similar to that normally found for C_{60}, except for the low-frequency shoulder at 1463 cm^{-1}, which is about 5 cm^{-1} higher than that reported for unexposed C_{60} samples.[28] The Raman spectrum (b) is typical of spectra taken in region (b) and shows a broadened and down-shifted line at 1447 cm^{-1} relative to that in region (a) (C_{60}). Finally the spectra in region (c) were of the form shown in trace (c) with a peak at 1430 cm^{-1}, in agreement with results shown for K_6C_{60} in Fig. 1. In accordance with previous work,[5] the spectrum (b) is identified with K_3C_{60}. Although the lines are broad, the results of Fig. 7 suggest the coexistence of stable phases for K_xC_{60} at C_{60}, K_3C_{60}, and K_6C_{60} rather than a continuous range of concentrations x. Similar conclusions have been reached by others.[12]

III. CONCLUSIONS

A comparison between the experimentally determined shifts in mode frequency arising from doping and the associated charge transfer with the calculations of Stanton and Newton[15] show that the modes that have a large amount of bond-bending displacements are shifted much more than the modes that involve predominately bond-stretching displacements. This finding implies that the A_u and some F_{1u} and H_u modes which involve major bond-bending displacements should experience relatively large mode frequency shifts. Some of these shifts should also be observable in the infrared spectra for the doped C_{60} samples.

Modes with predominantly radial displacements experience, in addition to the mode-softening effect associated with charge transfer, a mode-stiffening effect due to electrostatic interactions, which in some cases dominates over the mode-softening effect. These electrostatic interactions have two distinct origins: M^+-C_{60}^{6-} and a C_{60}^{6-} self-restoring interaction between the radial electric field from the $6e$ charge on the molecule and the surface charge distribution on the C_{60} shell.[27] Furthermore, the alkali-metal ions introduce an electrostatic interaction which further stiffens the mode frequency, and this effect is most pronounced for K_6C_{60} because of the smaller distance between the metal ion (M) and the C_{60} ball for M=K as compared with Rb and Cs.

All of the H_g modes of the C_{60} molecule would be expected to split in the lower T_h symmetry to E_g+T_g symmetry modes of solid C_{60} and its related metal-doped compounds. Only five of the H_g modes were found to split by measurable amounts. The two H_g modes with small splittings showed almost no polarization effects although the E_g and T_g modes should exhibit strong polarization properties. Three H_g modes with larger frequency splittings did show the anticipated polarization effects for the upper-frequency E_g component which softened much less than the lower-frequency component, presumably due to the relative dominance of bond-stretching displacements for the E_g component and bond-bending displacements for the T_g component.

Note added in proof. Since the submission of this manuscript several interesting and relevant papers have appeared on optically active vibrations in C_{60}-based solids. These results have been reviewed, and will appear in Ref. 33.

ACKNOWLEDGMENTS

The research at the University of Kentucky was funded in part by the University of Kentucky Center for Applied Energy Research and EPRI. The research at MIT was funded by NSF Grant No. DMR-88-19896. We gratefully acknowledge support for this research.

[1] W. Krätschmer, L. D. Lamb, K. Fostiropoulos, and D. R. Huffman, Nature **347**, 354 (1990).
[2] R.E. Haufler, J. J. Conceicao, L. P. F. Chibante, Y. Chai, N. E. Byrne, S. Flanagan, M. M. Haley, S. C. O'Brien, C. Pan, Z. Xiao, W. E. Billups, M. A. Ciufolini, R. H. Hauge, J. L. Margrave, L. J. Wilson, R. F. Curl, and R. E. Smalley, J. Phys. Chem. **94**, 8634 (1990).
[3] G. Meijer and D. S. Bethune, Chem. Phys. Lett. **175**, 1 (1990).
[4] G. Meijer and D. S. Bethune, J. Chem. Phys. **93**, 7800 (1990).
[5] R. C. Haddon, A. F. Hebard, M. J. Rosseinsky, D. W. Murphy, S. J. Duclos, K. B. Lyons, B. Miller, J. M. Rosamilia, R. H. Fleming, A. R. Kortan, S. H. Glarum, A. V. Makhiga, A. J. Muller, R. H. Eick, S. M. Zahurak, R. Tycko, G. Dabbah, and F. A. Thiel, Nature **350**, 320 (1991).
[6] M. J. Rosseinsky, A. P. Ramirez, S. H. Glarum, D. W. Murphy, R. C. Haddon, A. F. Hebard, T. T. M. Palstra, A. R. Kortan, S. M. Zahurak, and A. V. Makhija, Phys. Rev. Lett. **66**, 2830 (1991).
[7] A. F. Hebard, M. J. Rosseinsky, R. C. Haddon, D. W. Murphy, S. H. Glarum, T. T. M. Palstra, A. P. Ramirez, and A. R. Kortan, Nature **350**, 600 (1991).
[8] S. P. Kelty, C. C. Chen, and C. M. Lieber, Nature **352**, 223 (1991).
[9] K. Tanigaki, T. W. Ebbesen, S. Saito, J. Mizuki, J. S. Tsai, Y. Kubo, and S. Kuroshima, Nature **352**, 222 (1991).
[10] P. A. Heiney, J. E. Fischer, A. R. McGhie, W. J. Romanow, A. M. Denenstein, Jr., J. P. McCauley, and A. B. Smith III, Phys. Rev. Lett. **66**, 2911 (1991).
[11] J. E. Fischer, P. A. Heiney, A. R. McGhie, W. J. Romanow, A. M. Denenstein, Jr., J. P. McCauley, and A. B. Smith III, Science **252**, 1288 (1991).
[12] R. M. Fleming, A. P. Ramirez, M. J. Rosseinsky, D. W. Murphy, R. C. Haddon, S. M. Zahurak, and A. V. Makhija, Nature **352**, 787 (1991).
[13] R. M. Fleming, M. J. Rosseinsky, A. P. Ramirez, D. W. Murphy, J. C. Tully, R. C. Haddon, T. Siegrist, R. Tycko, S. H. Glarum, P. Marsh, G. Dabbagh, S. M. Zahurak, A. V. Makhija, and C. Hampton, Nature **352**, 701 (1991).
[14] O. Zhou, J. E. Fischer, N. Coustel, S. Kycia, O. Zhu, A. R. McGhie, W. J. Romanow, J. P. McCauley, Jr., A. B. Smith III, and D. E. Cox, Nature **351**, 462 (1991).
[15] R. E. Stanton and M. D. Newton, J. Phys. Chem. **92**, 2141 (1988).
[16] G. Meijer, D. S. Bethune, W. C. Tang, H. J. Rosen, R. D. Johnson, R. J. Wilson, D. D. Chambliss, W. G. Golden, H. Seki, M. S. DeVries, C. A. Brown, J. R. Salem, H. E. Hunziker, and H. R. Wendt, in *Clusters and Cluster-assembled Materials*, edited by R. S. Averback, J. Bernholc, and D. L. Nelson, MRS Symposia Proceedings No. 206 (Materials Research Society, Pittsburgh, 1991), p. 619.
[17] F. Negri, G. Orlandi, and F. Zerbetto, Chem. Phys. Lett. **144**, 31 (1988).
[18] Z. C. Wu, D. A. Jelski, and T. F. George, Chem. Phys. Lett. **137**, 291 (1987).
[19] D. E. Weeks and W. G. Harter, J. Chem. Phys. **90**, 4744 (1989).
[20] Ying Wang, J. M. Holden, A. M. Rao, Song-lin Ren, and P. C. Eklund, Phys. Rev. B **45**, 14 396 (1992). C. Reber, L. Yee, J. McKiernan, J. Zink, R. S. Williams, W. Tong, D. A. A. Ohlberg, R. L. Whetten, and F. Diederich, J. Phys. Chem. **95**, 2127 (1991).
[21] M. S. Dresselhaus and G. Dresselhaus, Adv. Phys. **30**, 139 (1981).
[22] K. A. Wang, Y. Wang, Ping Zhou, J. M. Holden, S. L. Ren, G. T. Hager, H. F. Ni, P. C. Eklund, G. Dresselhaus, and M. S. Dresselhaus, Phys. Rev. B **45**, 1955 (1992).
[23] R. A. Jishi and M. S. Dresselhaus, Phys. Rev. B **45**, 11 305 (1992).
[24] R. Al-Jishi and G. Dresselhaus, Phys. Rev. B **26**, 4523 (1982).
[25] J. Giergiel, P. C. Eklund, R. Al-Jishi, and G. Dresselhaus, Phys. Rev. B **26**, 6881 (1982).
[26] W. Andreoni, F. Gygi, and M. Parrinello (unpublished).
[27] R. A. Jishi and M. S. Dresselhaus, Phys. Rev. B **45**, 6914 (1992).
[28] S. J. Duclos, R. C. Haddon, S. H. Glarum, A. F. Hebard, and K. B. Lyons, Solid State Commun. **80**, 481 (1991).
[29] S. H. Tolbert, A. P. Alivisatos, H. E. Lorenzana, M. B. Kruger, and R. Jeanloz, Chem. Phys. Lett. **188**, 163 (1992).
[30] D. S. Bethune *et al.*, Chem. Phys. Lett. **179**, 181 (1991).
[31] P. Zhou, A. M. Rao, Kai-Am Wang, J. D. Robertson, C. Eloi, Mark S. Meier, S. L. Ren, Xiang-Xin Bi, P. C. Eklund, and M. S. Dresselhaus, Appl. Phys. Lett. **60**, 2871 (1992).
[32] G. Dresselhaus, M. S. Dresselhaus, and P. C. Eklund, Phys. Rev. B **45**, 6923 (1992).
[33] P. C. Eklund, Ping Zhou, Kai-Am Wang, G. Dresselhaus, and M. S. Dresselhaus, J. Phys. Chem. Solids (to be published).